Astron. Astrophys. 307, 635–644 (1996)

ASTRONOMY AND ASTROPHYSICS

Solar radiation pressure perturbations for Earth satellites

IV. Effects of the Earth's polar flattening on the shadow structure and the penumbra transitions

D. Vokrouhlický [1,2], P. Farinella [3], and F. Mignard [2]

[1] Astronomical Institute, Charles University, Švédská 8, 15000 Prague 5, Czech Republic
[2] Observatoire de la Côte d'Azur, Dept. CERGA, URA CNRS 1360, Av. N. Copernic, F-06130 Grasse, France
[3] Gruppo di Meccanica Spaziale, Dipartimento di Matematica, Università di Pisa, Via Buonarroti 2, I-56127 Pisa, Italy

Received 15 May 1995 / Accepted 18 July 1995

Abstract. We discuss the effects of taking into account the Earth's polar flattening when modelling the solar radiation force which perturbs the orbit of Earth satellites during their penumbra transitions. For this purpose, we generalize our previous theory for these perturbations (Vokrouhlický et al. 1993b), which assumed a spherical Earth. The new theory is then applied to two satellites for which the penumbra perturbations may produce detectable effects. The main changes with respect to the case with a spherical Earth appear in the timing of the transition phases leading from sunlight to shadow and *vice versa*, and in the overall duration of the eclipse intervals. These changes can cause short–periodic dynamical effects, and might be directly observable through *in situ* microaccelerometric measurements with good time resolution. On the other hand, we show that no additional long–term orbital effect on LAGEOS–type satellites is expected as a consequence of the Earth's polar flattening, owing to a symmetry in the shadow entry/exit phases, which causes the perturbations to average out along one satellite revolution.

Key words: celestial mechanics – artificial satellites, space probes – atmospheric effects

1. Introduction

In this series of papers, we have tried to develop in a rather systematical way a theory for the direct solar radiation pressure acting on artificial Earth satellites. The problem is complex (and interesting) especially during the so–called "penumbra transitions", when the satellite is about to enter into or exit from the Earth's shadow, so that the Earth's body and atmosphere partially absorb and/or refract the sunlight illuminating the satellite. The general background and motivations of this work have been outlined in Vokrouhlický et al. (1993b; Paper I), where a new method for the calculation of the radiation force has been described.

The penumbra phenomena can cause detectable effects on spacecraft trajectories over both long and short term. As for the short–periodic effects, these may be relevant to understand the source of some unmodelled perturbations on the GPS constellation satellites (Fliegel et al. 1992), as well as to analyse the data from future accelerometric missions which aim at carrying out *in situ* measurements of non–gravitational forces in space (Sehnal & Vokrouhlický 1994; Vokrouhlický 1994a and references therein). To a lesser extent, penumbra phenomena also affect the motion of satellites devoted to geodesy and geodynamics. In Paper II (Vokrouhlický et al. 1994a), we have discussed such effects in the framework of the analysis of the unmodelled residuals in LAGEOS' orbital evolution (see also Inversi & Vespe 1994).

The theory developed in Paper I was based on the assumption of a spherical shape of the Earth. Recently it has been pointed to us by some colleagues that the Earth's polar flattening might somewhat affect the results, and if so the corresponding corrections should be incorporated in the theory. The reason why such corrections cannot be discounted *a priori* as negligible is that according to Paper I the refraction of lightrays in the Earth's atmosphere proves to be crucial in determining the behaviour of the radiation force during penumbra transitions. Most of the relevant refraction effects take place in an atmospheric layer of just a few tens of km in thickness, quite comparable to the deviation of the Earth's figure from a perfect sphere. Thus one may wonder whether our refined model for the optical effects of the atmosphere is justified in view of the rough approximation for the Earth's global shape.

Therefore, we have decided to devote some work to the purpose of generalizing our theory to the case of a more realistic shape for the Earth, and to analyze the resulting discrepancies with respect to the spherical–Earth case. Of course, nothing is changed in the computation of the solar radiation force when the

Send offprint requests to: D. Vokrouhlický (Prague address), e-mail: davok@aci.cvut.cz

satellite is in full sunlight (see Sect. 3 in Paper I) or in complete shadow, and we will be concerned only with a more refined calculation of the Earth's shadow boundaries and of the force which is generated during the corresponding umbra/penumbra transitions. Since these perturbations are anyway small, we are going to model the Earth as an axisymmetric spheroid, neglecting its triaxiality (which is about three orders of magnitude smaller than the polar flattening). Moreover, in order to simplify the mathematical treatment, we will use as much as possible our previous spherical–Earth theory, by defining local spherical–like models for the atmosphere matching its global spheroidal shape. This constitutes a reasonable trade–off between rigor and tractability, because:

i) The Earth's polar flattening is relatively small and we expect that the theory developed for a spherical Earth provides a good zero–order approximation;

ii) The main effect of the Earth's non–spherical figure will be a slightly delayed or advanced occurrence of the penumbra transition, depending on the actual geometry of the satellite orbit, the orientation of the polar axis and the direction of the Sun, while the local structure of the atmosphere is not significantly affected by its global shape;

iii) This choice allows us to exploit most of the previously developed (and tested) software while dealing with the more general case.

We expect that such an extension of the theory will not significantly change our previous conclusions related to the long–term effects on LAGEOS, as they are described in Paper II. These perturbations were mainly caused by the asymmetry of the penumbra pattern between the shadow entry and exit, as a result of the large inclination of the orbit of LAGEOS combined with the annual climatic changes in the atmosphere. Such an asymmetry resulted into a nonzero component of the orbit–averaged transverse perturbation. As mentioned in item (ii) above, the dominant effect of the Earth's flattening is just a symmetrical advance or delay in the occurrence of the penumbra/umbra phenomena, without changing significantly the average value of the solar radiation force over one satellite revolution. As a consequence, most of the calculations developed below are relevant mainly for the short–periodic perturbations.

The remainder of this paper is organized as follows. In Sect. 2 we derive an eclipse condition including the effect of the Earth's polar flattening in the case of a purely geometrical shadow (no atmospheric effects — such models have been frequently used in orbit prediction/analysis software). Sect. 3 is the core of the paper and contains the additional mathematical tools needed to include in the theory the effects of the non–spherical figure of the Earth. (We remark that this paper uses extensively the formalism introduced in Paper I, which will be frequently referred to. Thus we advise the reader to have a look at Paper I before embarking on Sect. 3.) In Sect. 4 we illustrate some relevant examples in which the generalized theory is applied. Finally, Sect. 5 provides a short summary and conclusion.

2. Earth's flattening effects in modelling solar radiation pressure — the geometric approach

The easiest approach, and the most widely used, to model solar radiation pressure in numerical codes for orbit prediction and analysis is based on the assumption of sharp "step–like" passage across the boundary of the Earth's shadow zone (McCarthy 1992). The solar radiation field is represented as a homogeneous field with intensity related to the value of the solar constant. For a spherical Earth of radius $R_\oplus$ (not necessarily coinciding with the geometrical radius in this approximation; see McCarthy 1992), if we call r and ω the geocentric distance of the satellite and the geocentric angular distance of the satellite from the Sun, respectively, we have the following straightforward condition for the occurrence of an eclipse:

$$\left(\frac{R_\oplus}{r}\right)^2 > \sin^2\omega\,, \quad \cos\omega < 0\,, \tag{1}$$

which just corresponds to assuming that the satellite is located in the cylindrical shadow cast by the Earth, on the night side.

Consider now a more general situation with a non–spherical Earth. We assume that the boundary of the Earth is a well–defined convex surface (this is a basic assumption) and that the solar rays propagate along straight lines. Therefore the shadow occupies the interior of a quasi–cylinder defined by the surface with generators in the Sun–Earth direction. The satellite is in shadow when it is located in the night side of this quasi–cylinder.

Let $F(x\,,y\,,z) = 0$ be the equation of the surface of the Earth. In the following we will approximate this surface by an oblate spheroid with the major axis on the equatorial plane (twice the equatorial radius R_e) and a shorter polar axis (twice $R_p < R_e$). The flattening parameter is given by

$$f = \frac{R_e - R_p}{R_e} \tag{2}$$

and the equation of the surface can be written as

$$x^2 + y^2 + \frac{z^2}{(1-f)^2} = R_e^2\,.$$

If we call the satellite's radius vector from the centre of the Earth $\mathbf{r}$ and the unit vector toward the Sun $\mathbf{s}$, then we can split $\mathbf{r}$ into a component along $\mathbf{s}$ and another, $\mathbf{r}_\perp$, normal to $\mathbf{s}$ and lying in the plane defined by the Earth's centre, the Sun and the satellite. Then one has

$$\mathbf{r}_\perp = \mathbf{r} - (\mathbf{r}\cdot\mathbf{s})\,\mathbf{s}\,. \tag{3}$$

A necessary and sufficient condition for the satellite to be in the shadow zone is that the tip of the vector $\mathbf{r}_\perp$ starting at the centre of the Earth should be below the Earth's surface. Mathematically this means that if the components of $\mathbf{r}_\perp$ are $X\,,Y\,,Z$, one must have $F(X\,,Y\,,Z) < 0$.

By Eq. (3), this condition translates into:

$$F(x - u\,\sigma\,, y - v\,\sigma\,, z - w\,\sigma) < 0\,, \tag{4}$$

where $\sigma = \mathbf{r}\cdot\mathbf{s} = r\cos\omega$ and $\mathbf{s} = (u, v, w)$. In the case of a spheroid, condition (4) becomes:

$$(x-u\sigma)^2 + (y-v\sigma)^2 + \frac{(z-w\sigma)^2}{(1-f)^2} < R_e^2 \,, \tag{5}$$

or equivalently

$$(x-u\sigma)^2 + (y-v\sigma)^2 + (z-w\sigma)^2 - (z-w\sigma)^2\frac{f(2-f)}{(1-f)^2} < R_e^2 \,, \tag{6}$$

The first three terms reduce to $r^2\sin^2\omega$. With $z = r\cos\theta$ and $w = \cos\theta'$, one gets the conditions for an eclipse to occur as

$$\sin^2\omega - \frac{f(2-f)}{(1-f)^2}(\cos\theta - \cos\omega\cos\theta')^2 < \left(\frac{R_e}{r}\right)^2 \,, \quad \cos\omega < 0 \,, \tag{7}$$

where Eq. (1) is recovered with $f = 0$.

Other approaches include theories based on the occultation of the atmospherically undistorted solar disk behind the Earth (e.g. Métris 1986, Berlin 1988) or semi–analytical models based on the introduction of a shadow function (such as the one set forth by Ferraz–Mello 1964, 1972). Although we aim at developing a more refined theory, by no means we claim that these approaches are useless and should not be seen as more suitable in particular situations. We shall now move directly to the presentation of the full penumbra theory, including both the geometrical and the physical effects related to a spheroidal Earth figure.

3. Approximate theory for the penumbra effect

3.1. Mathematical technique and general principles

We systematically base our computations on the use of light rays (which describe all the *geometrical aspects* of light propagation), along which the radiative intensity is transported (thus conveying all the *physical aspects*). At any given point of the space (including the location of the satellite) we can thus construct a radiative field, defined by the intensity distribution. Then, in a separate step, the radiation pressure can be calculated taking into account the specific shape of a satellite as well as its orientation and surface properties.

In order to solve for the geometry of light rays, one needs to specify the refractive index κ everywhere between the light source (the Sun) and the satellite. We neglect refraction in the interplanetary medium, thus taking $\kappa = 1$ outside the Earth's atmosphere. Within the atmosphere, like in Paper I we adopt the model for the refraction of sunlight developed by Garfinkel (1944, 1967). Interestingly enough, in the case of a spherical Earth and a spherically stratified atmosphere, the geometry of the light rays can be handled analytically [see Paper I, Eqs. (23)–(28)]. This is an important point for concrete applications, as it considerably speeds up the evaluation of the radiative force.

As for the transport of the radiative intensity, the problem can be divided into two parts: (i) specification of the boundary conditions, (ii) specification of the propagation rules. For the boundary conditions in the solar photosphere, we resort to the Eddington solution for the solar limb–darkening, which allows one to set the value of the intensity according to the direction of emission. Although more refined solutions are now available, Eddington's one provides a good enough approximation for our needs. The intensity along the rays is obtained as a solution of the radiative transfer equations, and depends on the optical properties of the medium crossed by the light.

To stick to the theory developed for a spherical Earth, and considering that a more general treatment would be both very complex and irrelevant, we have adopted the following simplifying principle: *for any light ray reaching the satellite, we introduce an "osculating spherical Earth" with an "osculating spherically stratified atmosphere", which best approximate the actual conditions in the true atmosphere.*

Thanks to this trick, we can translate the whole light ray solution from the penumbra theory developed for the spherical Earth. The essence of the problem under consideration is then how to assign to a particular light ray and a particular point on this ray, an osculating spherical Earth and atmosphere. This point is elaborated upon in Sect. 3.3. It is worth noting that by this approximation we certainly account for the intuitively dominant effect of the Earth's flattening, i.e. the advanced/retarded occurrence of the beginning/end of the penumbra transition depending on the mutual configuration of the satellite, the Earth axis and the Sun. The mismodelled effects — non–planarity of light rays, departure of the osculating plane of the ray from the ellipsoid normal etc. — are supposed to be minor and neglected.

3.2. Geometrical tools

We will need below some classical geometrical results concerning the curvature of the ellipse and the intersection of an ellipsoid by a plane. They are briefly restated here for the sake of completeness. The parametric equations of an ellipse with semimajor axis a and eccentricity e are given by,

$$x = a\sin\lambda \quad , \quad y = a\sqrt{1-e^2}\cos\lambda \,,$$

where the parameter λ ranges in the interval $\langle 0, 2\pi\rangle$. At a point defined by λ the radius of curvature has the following form:

$$R_{\rm osc}(\lambda) = a\left(1-e^2\right)\left[\cos^2\lambda + \frac{\sin^2\lambda}{1-e^2}\right]^{3/2} \,, \tag{8}$$

Hence the coordinates of the centre of curvature are:

$$x_c(\lambda) = ae^2\cos^3\lambda \quad , \quad y_c(\lambda) = -a\frac{e^2}{\sqrt{1-e^2}}\sin^3\lambda \,. \tag{9}$$

Let us next consider the intersection of a spheroid by a plane. More in general, the intersection of a triaxial ellipsoid by a plane through its centre is an ellipse, since the the resulting equation is still of the second order and positive–definite. We will now determine the direction and size of the major and minor axes of this ellipse.

First we need the following result: any radius of a triaxial ellipsoid is less than the semimajor axis and more than the semiminor one. This is easily proved analytically with a little algebra, but can also be seen by a simple geometric argument. Such an ellipsoid is inscribed in a sphere with radius equal to the semimajor axis but circumscribes a sphere with radius equal to the semiminor axis. Therefore any radius is between these two extremes.

Now consider the plane (defined by its normal **N**) which goes through the origin, namely the centre of the spheroid. We assume the spheroid to be oblate with equatorial radius a and flattening parameter f. Any point (x, y, z) of the spheroid is such that

$$x^2 + y^2 + \frac{z^2}{(1-f)^2} = a^2 \,. \tag{10}$$

With the usual spherical coordinates (r, θ, ϕ), this becomes

$$r^2 \left[\sin^2\theta + \frac{\cos^2\theta}{(1-f)^2} \right] = a^2 \,. \tag{11}$$

The plane intersects the equator of the spheroid, so there is a radius of the ellipse drawn in the plane whose magnitude equals the equatorial radius of the spheroid, that is to say its semimajor axis. As no radius can be of greater magnitude, this is also the semimajor axis of the ellipse, which therefore lies along the line of intersection between the plane and the equator. Its magnitude is a and its direction is the same as the vector $\mathbf{N} \times \mathbf{k}$, where $\mathbf{k}$ is the unit vector directed toward the pole of the spheroid.

Now the minor axis of the ellipse is normal to both **N** and the semimajor axis and its vertex belongs to the spheroid. If the spherical coordinates of **N** are (Θ, Φ), then the semimajor axis vector is specified by $(a, \pi/2, \Phi + \pi/2)$ and the direction of the minor axis by $(\pi/2 - \Theta, \Phi + \pi)$. From Eq. (11), one gets the magnitude b of the semiminor axis as

$$b^2 \left[\cos^2\Theta + \frac{\sin^2\Theta}{(1-f)^2} \right] = a^2 \,, \tag{12}$$

or equivalently the eccentricity of the ellipse:

$$e^2 = \frac{f(2-f)\sin^2\Theta}{1 - f(2-f)\cos^2\Theta} \,. \tag{13}$$

With the axes of the spheroid a and c and b the minor axis of the ellipse, a more aesthetic form of Eq. (12) is

$$\frac{\cos^2\Theta}{a^2} + \frac{\sin^2\Theta}{c^2} = \frac{1}{b^2} \,. \tag{14}$$

Also, with $E^2 = f(2-f)$ for the eccentricity of the meridian section of the ellipsoid, one has for Eq. (13)

$$e^2 = \frac{E^2 \sin^2\Theta}{1 - E^2\cos^2\Theta} \,. \tag{15}$$

3.3. Approximate theory for the penumbra effects caused by a spheroidal Earth

As we are changing the basic geometrical assumption of the theory — using a spheroidal Earth model instead of a spherical one — it is clear that we must concentrate mainly on the geometrical aspects, that is on the light rays. Thus, the modelling of the extinction process remains the same as in Paper I, and we shall just summarize it briefly in Sect. 3.6.

We recall that a particular advantage of our method for the calculation of the geometrical aspects of photon trajectories in the Earth's atmosphere consists in the fact that we formulated (and analytically solved) the corresponding equations in a special plane — specified by the geocentric position vectors of the Sun and the satellite, and also called $\phi = 0$ slice plane (ϕ being a spherical angle in the satellite–bound local reference system introduced in Paper I). From the standpoint of the satellite, this plane corresponds to a particular (vertical) slice of the solar image. The behaviour of light rays which do not lie exactly in this plane has been proven to be identical to those in the $\phi = 0$ slice, provided several geometrical quantities (the Sun–Earth distance, the solar radius, the Sun–satellite geocentric angular distance) are properly redefined. We shall use this scheme also in this paper, so that our primary concern is to formulate the geometry of the light rays in the plane given by the geocentric position vectors of the Sun and the satellite.

The unit vector $\boldsymbol{N}(\Theta, \Phi)$ normal to the plane defined by the geocentric position vectors of the Sun $[\boldsymbol{n}(\vartheta', \varphi')]$ and the satellite $[\boldsymbol{n}(\vartheta, \varphi)]$ is given by

$$\sin\omega\, \boldsymbol{N}(\Theta, \Phi) = \boldsymbol{n}(\vartheta', \varphi') \times \boldsymbol{n}(\vartheta, \varphi) \,, \tag{16}$$

where ω is the geocentric angular distance between the Sun and the satellite and the angles Θ, Φ and alike refer to geocentric spherical coordinates. As mentioned in the previous section, the intersection of the Sun–satellite plane with the Earth body is an ellipse whose eccentricity is given by Eq. (13). We also define the auxiliary angles ι and ι' by the following transformation:

$$\cos\iota' = -\,|\sin\vartheta' \sin(\varphi' - \Phi)| \,, \tag{17a}$$

$$\cos\iota = |\sin\vartheta \sin(\varphi - \Phi)| \,, \tag{17b}$$

$$\sin\iota = \pm\sqrt{1 - \cos^2\iota} \,, \tag{17c}$$

where the plus sign in the last relation holds for $\iota + \iota' + \omega = 2\pi$ or $\iota' \geq \omega$, while the minus sign holds for $\iota + \iota' + \omega \neq 2\pi$ and $\iota' < \omega$. Geometrically, ι is the angle between the satellite and the semimajor axis of the ellipse drawn on the Earth (see Fig. 1).

Let us introduce now the osculating spherical Earth, which approximates the true Earth body in the vicinity of the grazing point G. We stress that this object is defined for each of the light rays in the Sun–satellite plane separately.

The angular distance of the grazing point G from the major axis of the ellipse defined on the Earth by the intersection of the Sun–satellite plane is parametrized by λ. Then the radius of the osculating Earth is given by Eq. (8), that is

$$R_\oplus(\lambda) = R_e(1-e^2)\left(\cos^2\lambda + \frac{\sin^2\lambda}{1-e^2} \right)^{3/2} \,, \tag{18}$$

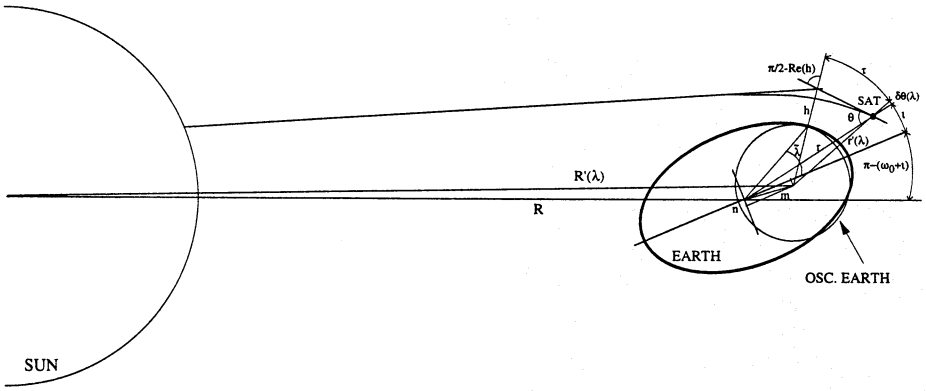

Fig. 1. Geometrical quantities in the Sun–satellite plane introduced in the text. Note the true intersection with the Earth body (bold–line ellipse) and the intersection with the osculating spherical Earth (thin–line circle). A particular light ray with local deflection θ (to which the osculating Earth belongs) is traced back to the emitter in the solar photosphere. Note the redefined geocentric solar and satellite distances R' and r' and the Sun–satellite geocentric angular distance ω', which is now referred to the centre of the osculating Earth. Compare with Fig. 2 of the Paper I where several supplementary angular parameters (α, β etc.) are given.

while Eq. (9) gives the cartesian coordinates of its centre:

$$m(\lambda) = R_e e^2 \cos^3\lambda \ , \quad n(\lambda) = -R_e \sin^3\lambda \frac{e^2}{\sqrt{1-e^2}} \ . \tag{19}$$

(note that these values apply to the system of axes rotated by the angle $\pi - \omega - \iota$ with respect to the axis given by the solar position — see Fig. 1).

Now what remains to be done is introducing the parameter λ in all the general formulae of Paper I, remembering that the centre of the pseudo–Earth is no longer coincident with the centre of the spheroid, but changes depending on the light ray (note the difference between the formal parameter λ and the geocentric angle $\tilde{\lambda}$ between the direction to a specified point on the Earth's surface and the direction of the Earth–cut major axis). Thus, hereinafter the geocentric distance of the Sun will become $R'(\lambda)$ instead of R and that of the satellite $r'(\lambda)$ instead of r, where "geocentric" will mean with respect to the centre of the osculating sphere. Likewise, the Sun–satellite geocentric angular distance is redefined as $\omega'(\lambda)$ instead of ω.

We recall our previous definitions

$$\rho_1 = \frac{R_\odot}{R} \quad , \quad \rho_2 = \frac{r}{R} \ , \tag{20}$$

to which we can formally add

$$\rho_3 = \frac{R_e}{R} \quad , \quad \rho_4 \left(= \frac{R}{R}\right) = 1 \ . \tag{21}$$

The parametrized counterparts of these quantities in the flattened Earth case are:

$$\rho_2'(\lambda) = \frac{r'(\lambda)}{R} \ , \quad \rho_3'(\lambda) = \frac{R_\oplus(\lambda)}{R} \ , \quad \rho_4'(\lambda) = \frac{R'(\lambda)}{R} \ , \tag{22}$$

using again primed letters to distinguish them from those applying to the spherical Earth case. We also define

$$\rho_m(\lambda) = \frac{m(\lambda)}{R} \quad , \quad \rho_n(\lambda) = \frac{n(\lambda)}{R} \ . \tag{23}$$

The last quantity which must be redefined for a particular light ray is the deflection $\theta' = \theta + \eta_\theta \delta\theta(\lambda)$ from the z–axis of the satellite–bound local frame. The parameter η_θ takes two possible values (± 1) and provides the sign of the angle $\delta\theta(\lambda)$. Note that one has to add it to the "true deflection" θ (as shown in Fig. 1) when the angle between the centre of the osculating Earth and the solar direction (measured in the clockwise sense) is greater than ω. In that case we define $\eta_\theta = +1$. When the angular distance between the centre of the osculating Earth and the Sun is smaller than ω, we have to subtract the variation $\delta\theta(\lambda)$ from the nominal value θ and thus $\eta_\theta = -1$.

Simple geometrical considerations lead to the following formulae:

$$\rho_2'^{\,2} = \rho_2^{\,2} + \rho_m^2 + \rho_n^2 - 2\rho_2 (\rho_m \cos\iota + \rho_n \sin\iota) \ , \tag{24}$$

$$\rho_4'^{\,2} = 1 + \rho_m^2 + \rho_n^2 - 2 [\rho_m \cos(\iota + \omega) + \rho_n \sin(\iota + \omega)] \tag{25}$$

and to

$$\cos\delta\theta(\lambda) = \frac{1}{\rho_2'} (\rho_2 - \rho_m \cos\iota - \rho_n \sin\iota) \ , \tag{26}$$

$$\cos\omega'(\lambda) = \frac{1}{\rho_2'\rho_4'} \Big\{ \rho_2 \cos\omega - \rho_m [\cos(\iota + \omega) + \rho_2 \cos\iota] - \rho_n [\sin(\iota + \omega) + \rho_2 \sin\iota] + \rho_m^2 + \rho_n^2 \Big\} \ . \tag{27}$$

All these quantities can be determined once the angle λ is known. With the help of Fig. 1 and a little algebra, the angle λ is determined from the following implicit equations

$$\cos\tilde{\lambda} = \frac{1}{\sqrt{\rho_3'^{\,2} + \rho_m^2 + \rho_n^2 + 2\rho_3' \upsilon}} \left\{ \rho_m + \frac{\rho_3'}{\rho_2'} \left[\rho_2 \cos(\tau + \iota) - \rho_m \cos\tau + \rho_n \sin\tau \right] \right\} \ , \tag{28}$$

$$\tan\tilde{\lambda} = \frac{1-f}{\sqrt{1 - f(2-f)\cos^2\Theta}} \tan\lambda \ , \tag{29}$$

where we have introduced the auxiliary quantities

$$\upsilon(\lambda,\theta,h)=\frac{1}{\rho_2'}\left\{\rho_2\left[\rho_m\cos(\tau+\iota)+\rho_n\sin(\tau+\iota)\right]-\rho_m^2\cos\tau-\rho_n^2\sin\tau\right\} \tag{30}$$

and

$$\tau(h,\theta,\lambda)=\frac{\pi}{2}+\mathrm{Re}[h,R_\oplus(\lambda)]-\theta-\eta_\theta\delta\theta(\lambda)\,. \tag{31}$$

Eq. (29) relates the formal parameter λ to the angle $\tilde{\lambda}$ appearing in Fig. 1. $\mathrm{Re}[h;R_\oplus(\lambda)]$ stands for the refraction angle of the light ray grazing the atmospheric layer at the altitude h. Eqs. (28)–(29) are not given in a closed form, since λ is hidden in the primed quantities. This basic set of equations together with the following Eqs. (32)–(34), already discussed in Paper I, relate all the important geometrical quantities for a given light ray, yielding a one–to–one correspondence between the surface elements E on the solar photosphere and the direction of emission β with respect to the normal direction.

Now the bending of the light ray is related to the refractive index $\kappa(h,\lambda)$ by

$$\rho_2'(\lambda)\sin[\theta+\eta_\theta\delta\theta(\lambda)]=\left[\rho_3'(\lambda)+\frac{h}{R}\right]\kappa(h,\lambda)\,, \tag{32}$$

In the case of Garfinkel's model of the Earth atmosphere we have

$$\kappa(h,\lambda)=1+a_0\left[1-2\gamma^2\frac{h}{R_\oplus(\lambda)+h}\right]^n\,, \tag{33}$$

where (a_0,γ) are model parameters and n is the polytropic index of the air. We recall that the top of this assumedly polytropic atmosphere is given by $h_\mathrm{T}(\lambda)=R_\oplus(\lambda)(2\gamma^2-1)^{-1}\approx(n+1)\mathscr{R}T_0/g_0$, where $\mathscr{R}$ is the gas constant for the air, T_0 and g_0 the temperature and gravity at the bottom of the atmosphere. The atmospheric height is primarily dependent on T_0 and to a lesser extent on the radius of the osculating Earth $R_\oplus(\lambda)$; the dependence on the gravity field g_0 is very small. Finally the ray geometry is determined by the equations:

$$\rho_1\sin\sigma=\rho_4'(\lambda)\sin(\sigma+\alpha)\,, \tag{34a}$$

$$\rho_2'(\lambda)\sin[\theta+\eta_\theta\delta\theta(\lambda)]\;\sin\sigma=\eta_1\rho_4'(\lambda)\sin\alpha\sin\left(\sigma+\eta_2\beta\right)\,, \tag{34b}$$

$$\beta=\eta_2\left(\alpha-\eta_1\xi\right)\,, \tag{34c}$$

where

$$\xi(\theta,\lambda)=\pi+2\mathrm{Re}[h;R_\oplus(\lambda)]-\omega'(\lambda)-\theta-\eta_\theta\delta\theta(\lambda)\,.$$

Here, (η_1,η_2) are auxiliary quantities having values ±1, as defined in Paper I. Eqs. (28)–(29), (32)–(34) together with the previous definitions form an algebraically intricate system linking the quantities $(\alpha,\beta,\sigma,\theta,h;\lambda,\tilde{\lambda})$. Note that this list contains more parameters than the number of the equations. This is due to the fact that in practice we always fix some of these quantities solving for the other ones, depending on the nature of the problem. We shall now give some examples of this (more details can be found in Paper I).

3.4. Phases of the penumbra transition

As in Paper I, we can distinguish five different phases between full sunlight and complete shadow: *phase 0*: out of shadow; *phase I*: partial atmospheric penumbra; *phase II*: full atmospheric penumbra; *phase III*: true penumbra with part of the solar disk covered by the solid Earth's horizon: *IV*: full umbra. During these phases the instantaneous position of the satellite can be specified through ω, the geocentric Sun–satellite angular distance. For example, the onset of phases (*I* and *II*) is obtained by solving first iteratively Eqs. (28)–(29) for the parameter $\lambda=\lambda_1$ with

$$\tau(\lambda)=\frac{\pi}{2}-\arcsin\left\{\rho_2'^{-1}(\lambda)\left[\rho_3'(\lambda)+\frac{h_\mathrm{T}(\lambda)}{R}\right]\right\}\,. \tag{35}$$

Then two auxiliary quantities $\omega_{\mathrm{A}1}$ and $\omega_{\mathrm{A}2}$ (generalizing the corresponding parameters in Paper I) are computed as

$$\omega_{\mathrm{A}1}=\frac{\pi}{2}-\Lambda_+(\Psi_T;r,R_\odot,R,\lambda_1)\,, \tag{36}$$

$$\omega_{\mathrm{A}2}=\frac{3\pi}{2}-\Lambda_-(\Psi_T;r,R_\odot,R,\lambda_1)\,, \tag{37}$$

where $\Psi_\mathrm{T}=\Psi[h_\mathrm{T}(\lambda_1),\lambda_1]$ and

$$\Lambda_\pm(\Psi;r,R_\odot,R,\lambda)\equiv\arcsin\left\{\frac{\Psi}{r}\frac{\rho_2}{\rho_2'\rho_4'}\left(\rho_1\pm\frac{\Psi}{R}\right)\mp\sqrt{\left[1-\left(\frac{\rho_2}{\rho_2'}\frac{\Psi}{r}\right)^2\right]\left[1-\frac{1}{\rho_4'^2}\left(\rho_1\pm\frac{\Psi}{R}\right)^2\right]}\right\}\,, \tag{38}$$

$$\Psi(h,\lambda)\equiv(R_\oplus+h)\,\kappa(h,\lambda)\,. \tag{39}$$

We are in phase *0* when $\omega<\omega_{\mathrm{A}1}$ whereas the phase *I* occurs when $\omega_{\mathrm{A}1}\le\omega<\omega_{\mathrm{A}2}$.

In a similar way, the conditions for the occurrence of phases *III* and *IV* are found by solving Eq. (28) for the parameter $\lambda=\lambda_2$ with

$$\tau(\lambda)=\frac{\pi}{2}+\mathrm{Re}\left[0;R_\oplus(\lambda)\right]-\arcsin\left\{\rho_2'^{-1}(\lambda)\rho_3'(\lambda)\,(1+a_0)\right\}\,. \tag{40}$$

Then the following quantities must be computed:

$$\omega_\mathrm{P}=\frac{\pi}{2}+2\mathrm{Re}[0;R_\oplus(\lambda_2)]-\Lambda_+(\Psi_0;r,R_\odot,R,\lambda_2)\,, \tag{41}$$

$$\omega_\mathrm{S}=\frac{3\pi}{2}+2\mathrm{Re}[0;R_\oplus(\lambda_2)]-\Lambda_-(\Psi_0;r,R_\odot,R,\lambda_2)\,. \tag{42}$$

Here $\Psi_0=\Psi[0;R_\oplus(\lambda_2)]$. Eventually we get the boundaries for the penumbra/umbra phases: phase *II* for $\omega_{\mathrm{A}2}\le\omega<\omega_\mathrm{P}$, phase *III* for $\omega_\mathrm{P}\le\omega<\omega_\mathrm{S}$ and phase *IV* for $\omega_\mathrm{S}\le\omega$.

3.5. The image of the distorted Sun

A piece of important information to be determined from the light ray geometry equations are the θ–limits of the solar image in the local satellite–bound, Sun–oriented reference frame. This is the most cumbersome geometrical task, as we have to solve Eqs. (28), (32) and the following equation (43) for a set of

three parameters (λ, h, θ). From Eqs. (34) by fixing a constraint $\beta = \pi/2$ we obtain

$$\sin\left[\theta + \eta_\theta \delta\theta\,(\lambda)\right] = \zeta^{-1}\left(\cos\varpi, \rho_2'/\rho_4'\right)\left[\eta_1 \rho_1 \rho_4'^{-2}\left(\rho_2' - \rho_4'\cos\varpi\right) + \sin\varpi\sqrt{\zeta\left(\cos\varpi, \rho_2'/\rho_4'\right) - (\rho_1/\rho_4')^2}\right], \quad (43)$$

$$\varpi(h,\lambda) = \omega'(\lambda) - 2\mathrm{Re}[h; R_\oplus(\lambda)],$$

$$\zeta(x,\alpha) \equiv 1 + \alpha^2 - 2x\alpha .$$

The parameter η_1 takes values of +1 and −1 when determining the upper an lower limb, respectively, giving θ_+ and θ_-. It is an easy task to eliminate $[\theta + \eta_\theta \delta\theta(\lambda)]$ using either Eq. (43) or Eq. (32). The remaining two equations to be solved for the parameters (λ, h) cannot be expressed in a simple algebraic form and have to be handled together. We have developed a fast iterative procedure to get the two roots (λ_3, h_3). Then, one can finally determine the two θ–limits of the solar image and define its apparent vertical width $\Delta\theta = (\theta_+ - \theta_-)$.

Up to now, we have considered the solution in the plane defined by the geocentric directions of the Sun and the satellite. An important property of this solution is that solutions in other "misaligned" planes (parametrized by the spherical angle ϕ in the satellite–bound local frame) are closely related to it. The only difference is that a few quantities have to be properly redefined. The normal vector $\boldsymbol{M}(\Theta, \Phi)$ to the plane of interest generalizing the previous $\boldsymbol{N}(\Theta, \Phi)$ is given by

$$\boldsymbol{M}(\Theta,\Phi) = \cos\phi\,\boldsymbol{N} - \frac{\sin\phi}{\sin\omega}\left[\cos\omega\,\boldsymbol{n}\,(\vartheta,\varphi) - \boldsymbol{n}\,(\vartheta',\varphi')\right], \quad (44)$$

where $\boldsymbol{n}(\vartheta,\varphi)$ and $\boldsymbol{n}(\vartheta',\varphi')$ remain the same as before. Simple geometrical arguments also show that the solar radius $R_\odot$ should be rescaled to the value of $R_\odot(\phi) = R_\odot\left(1 - \rho_1^{-2}\sin^2\phi\sin^2\omega\right)^{1/2}$, whereas the geocentric distance to the Sun must be rescaled to $R(\phi) = R\left(1 - \sin^2\phi\sin^2\omega\right)^{1/2}$. In the same manner, one shows that the geocentric angular distance between the satellite radius vector and the Sun must be rescaled to $\cos\omega(\phi) = \cos\omega\left(1 - \sin^2\phi\sin^2\omega\right)^{-1/2}$. The procedure to compute the geometrical properties of the light rays in the generic ϕ–slice thus consists in redefining all of these quantities, as a first step. Then, all the other derivations valid in the $\phi = 0$ plane can be applied. The ϕ–width of the solar image in the satellite–bound local frame $\phi_{\max} = \arcsin\left(\rho_1 \sin^{-1}\omega\right)$ remains the same in the ϕ–plane.

3.6. The geometrical flux attenuation and the Rayleigh extinction

The last point of this section concerns the modelling of other physical processes (in particular the Rayleigh extinction) occurring in the Earth's atmosphere. Once the osculating Earth has been defined by the procedure described above, we can apply the scheme discussed in Sect. 4.2 of Paper I without any change. Basically, we adopt a two–stage procedure: first only the geometrically induced attenuation of the radiative fluxes with constant radiative intensity along the individual light rays is considered. Then the true physical extinction is modelled by an exponential damping proportional to the optical depth along the light ray. In the latter case, the decrease of the density in the Earth's (polytropic) atmosphere is taken into account.

3.7. Derivation of the radiative force

As in the previous papers of this series, the final step is the computation of the radiation force acting on the satellite from the radiative flux vector, that is

$$\mathbf{F} = \int_{(\theta,\phi)} d(\cos\theta)d\phi\;\boldsymbol{n}(\theta,\phi)\,I(\theta,\phi)\,. \quad (45)$$

The integration is performed over the radiative field $I(\theta,\phi)$ impinging on the satellite (of course, this can also as an integration over the distorted solar image observed in the satellite–bound local frame). The radiative force is directly proportional to the flux vector (45) in the case of a spherical satellite (Vokrouhlický et al. 1993a). This is a fairly good approximation for LAGEOS. We have applied the same approximation also to the case of the CESAR satellite (to be equipped with the MACEK accelerometer; see later), despite its more complex shape. The main reason is that we wanted to avoid mixing the effects induced by the Earth's flattening with those due to the satellite geometry, which can be treated independently (see Vokrouhlický 1994b).

4. Applications

As in the previous papers of this series, we apply the theory developed in this paper to some concrete cases in which it may prove relevant. We are going to deal with two satellites, LAGEOS and CESAR. The former one is an example of an existing geodesy/geodynamics satellite orbiting at intermediate altitude ($\approx$ 5500 km), whereas the latter one is a planned accelerometric spacecraft to be be inserted into a low orbit, a few hundred km above the Earth's surface. The pattern of penumbra phenomena is somewhat different in the two cases (see Paper I), in part because of the difference in orbital speed and in part as a result of the different angular extent of the Earth's atmosphere as "seen" from the satellite.

In order to assess the effects of the Earth's flattening we have compared the results obtained either taking it into into account or not in the model for the computation of the radiation force. Of course, at the same time we have checked that the spherical–Earth results agree with those obtained in Paper I, where we had used a (partially) independent software.

4.1. Results for the CESAR satellite

The CESAR satellite is planned for launch into a low–altitude orbit with a semimajor axis of about 7100 km, an eccentricity of 0.04 and an inclination 70°. A highly sensitive accelerometer (MACEK) will be carried on–board to perform instantaneous measurements of the non–gravitational forces acting on

the satellite (Sehnal & Vokrouhlický 1994). The time resolution of the MACEK measurements will be roughly 2 seconds, with a sensitivity of about 5×10^{-10} m s^{-2} (R. Peřestý, private communication). At such levels of time resolution and sensitivity we show conclusively that the slight modification of the radiation pressure force brought about by the Earth's non–spherical shape should be accounted for in the analysis of MACEK data.

In order to get a clearer picture of the effects of the Earth's flattening on the radiation force in low orbits we consider two possible inclinations, 90° and 60° respectively. In our first run, we put the Sun on the Earth's equator and in the orbital plane of the satellite (in other words, either $\Omega = \lambda_\odot$ or $\Omega = \lambda_\odot + \pi$). With the inclination set at 90°, the orbital configuration minimizes the duration of the penumbra transition, because the satellite enters (or exits) the penumbra region in the normal direction. Fig. 2a shows the results for this case.

Solid curves are derived from the spheroidal Earth model (with the true flattening parameter f), while the dashed ones correspond to the spherical Earth model (with the radius equal to the equatorial one in case of the oblate Earth, i.e., we just formally put $f = 0$ in the theory). In either case, we assumed "normal atmospheric conditions" as defined by Garfinkel (1967). The most significant feature is the delayed onset of the penumbra in the spheroidal Earth case, as a result of the smaller diameter of the shadow zone in the polar direction than in the equatorial one. In Fig. 2a, this shows up as an time shift (the origin of the time axis has been fixed at the beginning of the penumbra phase in the oblate Earth case). Although a more detailed analysis shows that the Earth flattening effect cannot be completely reduced to a simple time shift (this fact is better seen in the following Fig. 2b, where the relative configuration of the Earth, the Sun and the satellite orbit has been changed), the approximate extent of the time shift observed in Fig. 2a (and 3a, see later) can be estimated by simple geometrical arguments as

$$\Delta T \approx \frac{\Delta h}{n R_e \sqrt{(r/R_e)^2 - 1}} , \qquad (46)$$

where n is the satellite's mean motion and Δh is the difference between the equatorial and polar radii of the Earth. For the CESAR satellite one gets $\Delta T \approx 7$ s, in good agreement with the numerical results. Similarly, for the LAGEOS satellite we obtain $\Delta T \approx 5$ s, a good match for the result of the corresponding numerical run (Fig. 3a).

In the second run, the orbital plane is rotated by 90°, so that $\Omega = \lambda_\odot + \pi/2$, and the inclination is reduced to about 60°, so that the orbit just grazes the quasi–cylindrical Earth's shadow. This orbits is closer to that foreseen for CESAR. Moreover, as discussed in Paper II, such a grazing configuration maximizes the differences between the refined models of the penumbra and those neglecting atmospheric refraction. Fig. 2b shows that the results in this case are qualitatively similar to those of Fig. 2a. However, as expected, the Earth flattening effects are quantitatively much larger in this case. Thus the CESAR data analysis would be significantly degraded if the Earth flattening effects were not properly accounted for in the computation of the solar radiation force.

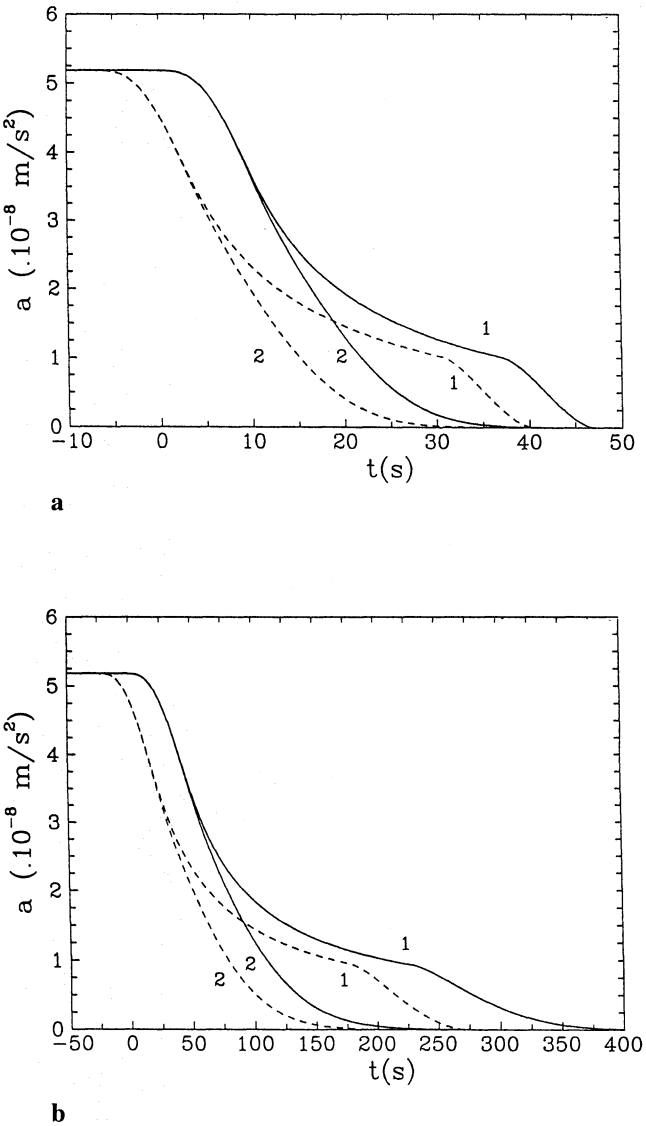

Fig. 2a and b. Amplitude (a) of the solar radiation pressure acceleration vs. time (t, in seconds) since the beginning of the penumbra transition in the case of the (low–altitude) CESAR satellite. Parts **a** and **b** correspond to the two different Sun vs. satellite orbit configurations discussed in the text. Solid curves correspond to the spheroidal Earth model with $f = 1/298.28$, and dashed curves to a spherical Earth model. Labels 1 and 2 refer to the presence or absence of atmospheric extinction, respectively. Ordinate units are 10^{-8} m/s^2.

4.2. Results for the LAGEOS satellite

We have performed a similar analysis in the case of LAGEOS, which orbits the Earth at a much higher altitude. The corresponding results are plotted in Figs. 3a and 3b. We can again conclude that the most important consequence of the Earth's flattening is an earlier/later onset of the penumbra phenomenon, with a somewhat shorter time shift for the reasons discussed above (and a longer penumbra transition, as already found in Paper I). The fact that a delayed entrance into penumbra is par-

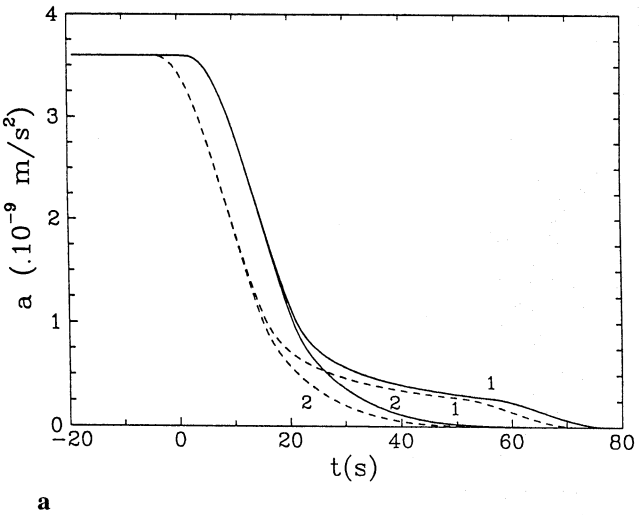

a

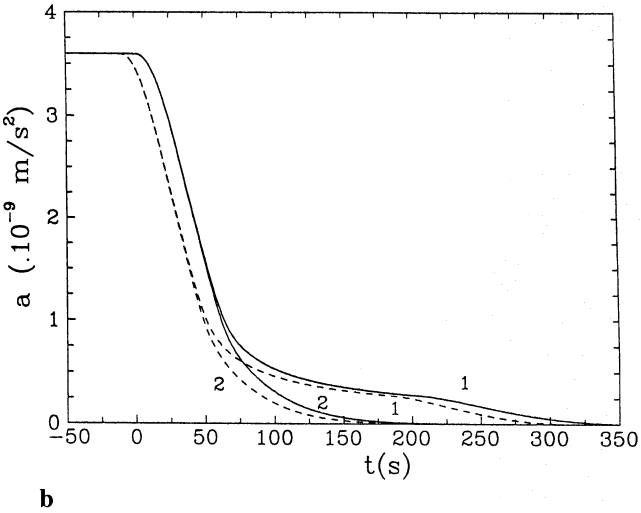

b

Fig. 3a and b. The same as in Figs. 2 but for the (higher–altitude) LAGEOS satellite. Ordinate units have been changed to 10^{-9} m/s^2.

alleled by a symmetric advance of the exit from it suggests that the Earth's flattening effects do not contribute significantly to the long–term perturbations studied in Paper II. However, since the shift of the eclipse conditions does not operate in the same sense at the shadow entry and exit, there is a net shortening of the eclipse interval (of the order of 15–20 seconds for the true LAGEOS orbit). This means that for the analysis of short–term perturbations on LAGEOS orbit, the Earth flattening phenomena discussed in this paper may become more important than the short–term perturbations related to the penumbra effect itself, as treated in Papers I and II. However, for LAGEOS the corresponding displacement should remain below the measurable threshold with current SLR technology (about 1 cm).

Let us now address in a more direct way the long–term perturbations. To investigate the effect of the Earth's flattening on the long–term along–track perturbing acceleration acting on

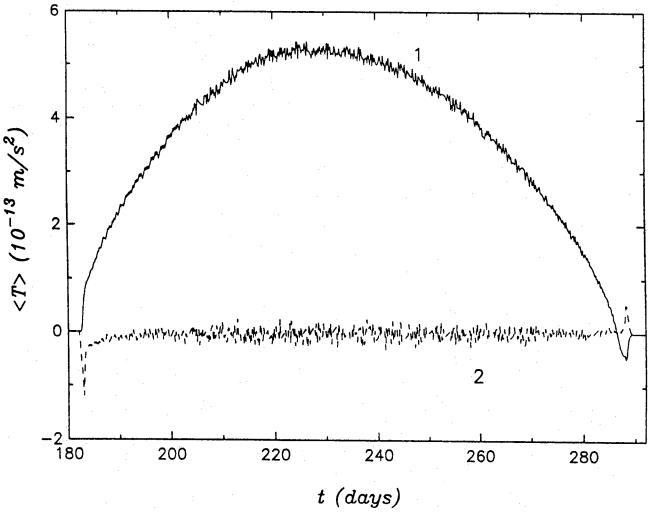

Fig. 4. Difference in the orbit–averaged along–track acceleration of LAGEOS I between a model with a spherical Earth and one allowing for polar flattening. Time is in days, starting at launch. Curve 1 shows the acceleration due to the penumbra effect and and curve 2 the difference between the two models. Accelerations are in 10^{-13} m s^{-2}.

LAGEOS we have repeated some of the computations described in Paper II, but using the oblate Earth model developed here. On order to do this efficiently, we have relied on a simplified version of the full penumbra theory, along the same lines as discussed in Paper II. In particular:

i) the double integration of Eq. (45) is reduced to a single one by omitting the ϕ–dimension;
ii) the magnitude of the perturbative force is estimated by multiplying the force computed just before the onset of the penumbra transition times a factor giving the vertical compression of the solar disk (to account for refraction) and times the exponential damping parameter which accounts for absorption, averaged over the vertical slice of the solar image seen in the satellite local frame;
iii) the direction of the radiation force is determined by the light ray emitted from the effective centre of the solar disk image [$\beta = \pi/2$ in Eqs. (34)].

In Fig. 4, curve 2 shows the change in the acceleration due to the penumbra phenomenon depending on whether the flattening effect is included in the model or not. The net signal predicted by our simplified theory is shown by curve 1 and should be compared with Fig. 4b in Paper II. We have selected the first interval after the launch of LAGEOS I when the shadow–crossing condition was fulfilled and kept the same model for the seasonal and latitudinal variations of the meteorological parameters at the bottom of the atmosphere as in Paper II. We remark that the difference represented by curve 2 is at least one order of magnitude smaller than the signal itself (which reaches up to $\approx 5 \times 10^{-13}$ m s^{-2}), and therefore can be safely neglected in the analysis of LAGEOS data. The spikes just at the beginning and at the end of the shadow–crossing interval are due to transient effects in the numerical averaging over the first and the last orbit included in this interval.

5. Conclusions

The main results obtained in this paper can be summarized as follows:

1. We have generalized our previous scheme for modelling the perturbing forces on artificial satellites arising from solar radiation pressure during the passages from the full sunlight to complete shadow (and *vice versa*). A spheroidal model of the Earth's shape with an arbitrary flattening coefficient is used instead of a simple spherical model. We have shown by a series of examples that no major difference appears between a model assuming a spherical Earth and a more realistic one including polar flattening. The most obvious change appears in the timing of the penumbra phases leading from the full sunlight into darkness and *vice versa*, with a time shift effect which can be easily explained by geometric arguments. It appears worth accounting for this tiny effect when dealing with data provided either by geodetic satellites, because of the improving quality of orbital tracking, or by future microaccelerometric experiments dedicated to *in situ* measurements of non–gravitational forces. (One such mission is being currently prepared by the Ondřejov research team; see Sehnal & Peřestý 1992 and Sehnal & Vokrouhlický 1994). Also, some short–periodic perturbation terms might be mismodelled when the Earth flattening effect is not considered in the evaluation of the radiation forces.

2. A special attention has been devoted to the possible role of the penumbra effect in the analysis of the long–term evolution of the orbit of LAGEOS. The tests performed in this paper, although of limited scope, indicate that our previous results based on a spherical Earth model are still valid. The reason is that the main feature affecting the long–term effects (that is, after averaging the perturbations over one orbital period) is the asymmetry of the perturbing acceleration pattern between entry in, and exit from shadow. However, the introduction of a spheroidal Earth does not modify significantly this asymmetry, and thus leaves the long–term perturbations unchanged. Of course, for the real Earth some global asymmetry is associated to the pear—like shape of the geoid, as represented e.g. by the J_3 term in its spherical harmonics expansion. But quantitatively this effect is of the order of 50 m (Vaníček & Krakiwsky 1992), which is quite negligible with respect to the spheroidal flattening and also to the meteorologically induced optical asymmetry analysed in Paper II.

Acknowledgements. We are grateful to D. Lucchesi and A. Milani for useful discussions, and to P. Exertier for some help in drawing Fig. 1. D.V. has worked to this paper while staying at the Observatoire de la Côte d'Azur (Dept. CERGA, Grasse, France) thanks to the "H. Poincaré" research fellowship, partially funded by the General Council of the Alpes Maritimes. He is also grateful to the University of Pisa for its kind hospitality. P.F. acknowledges support from the Italian Space Agency (ASI) and from the Italian Ministry for University and Scientific Research (MURST).

Appendix A

In this appendix, we wish to correct a few misprints which appeared in previously published papers of the current series, devoted to solar radiation pressure perturbations. We apologize for these errors to any colleague who might have tried to apply our penumbra theory.

In Paper I (Vokrouhlický et al. 1993b), one should replace $\rho_2(\phi)$ with r in Eq. (37), so that the correct equation reads

$$\Psi\left[h\left(\theta,\phi\right)\right] = r\sin\theta\ . \tag{37}$$

In the same paper, labels 2 and 3 should be interchanged in Fig. 14 (we thank R. Hujsak for pointing this error to us). Also, the law for "rescaling" the Sun–satellite geocentric angular distance, mentioned at p. 303, has been mistyped. The correct equation reads

$$\cos\omega(\phi) = \cos\omega\left(1-\sin^2\phi\sin^2\omega\right)^{-1/2}\ .$$

References

Berlin P., 1988, The Geostationary Applications Satellite, Cambridge Univ. Press, Cambridge
Ferraz–Mello S., 1964, C.R. Acad. Sci. Paris 258, 463
Ferraz–Mello S., 1972, Celest. Mech. 5, 80
Fliegel H.F., Gallini T.E., Swift E.R., 1992, J. Geophys. Res. 97, 559
Garfinkel B., 1944, AJ 50, 169
Garfinkel B., 1967, AJ 72, 235
Inversi P., Vespe F., 1994, Adv. Space Res. 14, (5)73
McCarthy D.D. (ed.), 1992, IERS Standards (1992), IERS Technical Note T13, Observatoire de Paris
Métris G. 1986, Contribution à la modélisation de haute précision des effects de la pression de radiation solaire sur les trajectoires des satellites artificiels, Memoire de diplome d'ingegneur, Ecole Nationale Superieure, Strasbourg
Milani A., Nobili A.M., Farinella P., 1987, Non–Gravitational Perturbations and Satellite Geodesy, Hilger, Bristol
Milani A., Carpino M., Rossi A., Catastini G., Usai S., 1995, Manuscripta Geod. 20, 123
Sehnal, L., Peřestý, R., 1992, in: Geodesy and Physics of the Earth, Proc. IAG Symposium No. 112, p. 129, Springer Verlag, Berlin
Sehnal L., Vokrouhlický D. 1995, Adv. Space Res. 16, in press
Seidelmann, P.K. (ed.), 1992, Explanatory Supplement to the Astronomical Almanach, Univ. Science Books, Mill Valley
Vaníček P., Krakiwsky E., 1992, Geodesy: The Concepts, Elsevier, Amsterdam
Vokrouhlický D., 1994a, Publ. Astron. Inst. Ondřejov 82, 16
Vokrouhlický D., 1994b, Publ. Astron. Inst. Ondřejov, submitted
Vokrouhlický D., Farinella P., Lucchesi D., 1993a, Celest. Mech. 57, 225
Vokrouhlický D., Farinella P., Mignard F., 1993b, A&A 280, 295 (Paper I)
Vokrouhlický D., Farinella P., Mignard F., 1994a, A&A 285, 333 (Paper II)
Vokrouhlický D., Farinella P., Mignard F., 1994b, A&A 290, 324 (Paper III)

This article was processed by the author using Springer-Verlag TEX A&A macro package 1992.